Journal of Power Sources 301 (2016) 219–228

Contents lists available at ScienceDirect

Journal of Power Sources

journal homepage: www.elsevier.com/locate/jpowsour

One-step electrosynthesis of ethylene and ethanol from CO_2 in an alkaline electrolyzer

Sichao Ma [a, b], Masaaki Sadakiyo [b, c], Raymond Luo [a], Minako Heima [b, c], Miho Yamauchi [b, c, **], Paul J.A. Kenis [a, b, *]

[a] School of Chemical Sciences, University of Illinois at Urbana-Champaign, 505 South Mathews Ave, Urbana, IL 61801, USA
[b] International Institute for Carbon-Neutral Energy Research (WPI-I2CNER), Kyushu University, 744 Moto-oka, Nishi-ku, Fukuoka 819-0395, Japan
[c] CREST, JST, 4-1-8 Honcho, Kawaguchi, Saitama 332-0012, Japan

HIGHLIGHTS

- One-step electroreduction of CO_2 to C2 products achieved using Cu nanoparticles.
- 10× current density for C2 products vs. prior work obtained at only −0.58 V.
- High performance when using a GDE with rough catalyst in alkaline electrolyte.
- Morphology rather than oxidation levels of catalysts affects product distribution.
- GDEs covered with Cu nanoparticles remain stable over 4-h electrolysis.

GRAPHICAL ABSTRACT

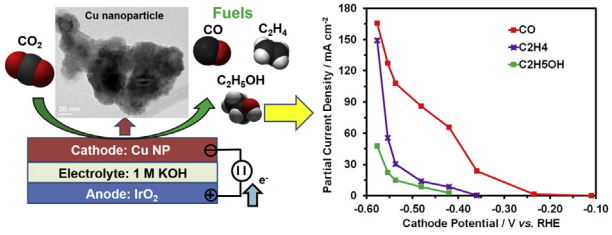

ARTICLE INFO

Article history:
Received 2 July 2015
Received in revised form
14 September 2015
Accepted 29 September 2015

Keywords:
CO_2 reduction
Cu nanoparticles
C2 hydrocarbons
Alkaline electrolyzer
Carbon-neutral energy

ABSTRACT

Electroreduction of CO_2 has potential for storing otherwise wasted intermittent renewable energy, while reducing emission of CO_2 into the atmosphere. Identifying robust and efficient electrocatalysts and associated optimum operating conditions to produce hydrocarbons at high energetic efficiency (low overpotential) remains a challenge. In this study, four Cu nanoparticle catalysts of different morphology and composition (amount of surface oxide) are synthesized and their activities towards CO_2 reduction are characterized in an alkaline electrolyzer. Use of catalysts with large surface roughness results in a combined Faradaic efficiency (46%) for the electroreduction of CO_2 to ethylene and ethanol in combination with current densities of ~200 mA cm^{-2}, a 10-fold increase in performance achieved at much lower overpotential (only < 0.7 V) compared to prior work. Compared to prior work, the high production levels of ethylene and ethanol can be attributed mainly to the use of alkaline electrolyte to improve kinetics and the suppressed evolution of H_2, as well as the application of gas diffusion electrodes covered with active and rough Cu nanoparticles in the electrolyzer. These high performance levels and the gained fundamental understanding on Cu-based catalysts bring electrochemical reduction processes such as presented here closer to practical application.

* Corresponding author. Department of Chemical & Biomolecular Engineering, University of Illinois at Urbana-Champaign, 600 South Mathews Avenue, Urbana, IL 61801, USA.
** Corresponding author. International Institute for Carbon-Neutral Energy Research (WPI-I2CNER), Kyushu University, 744 Moto-oka, Nishi-ku, Fukuoka 819-0395, Japan.
E-mail addresses: yamauchi@i2cner.kyushu-u.ac.jp (M. Yamauchi), kenis@illinois.edu (P.J.A. Kenis).

http://dx.doi.org/10.1016/j.jpowsour.2015.09.124
0378-7753/

1. Introduction

Prior work suggests that multiple approaches including switching to renewable energy sources, increasing energy efficiency of buildings, increasing the fuel efficiency of vehicles, and applying underground carbon sequestration need to be implemented at a large scale in order to significantly reduce global CO_2 emissions, which, in turn, may help curb the undesirable effects of climate change [1–4]. Another approach, the electrochemical reduction of CO_2 to various value-added chemicals such as carbon monoxide (CO), formate ($HCOO^-$), methane (CH_4), ethylene (C_2H_4) and alcohols offers promise to suppress CO_2 emissions while it at the same time utilizes excess electrical energy from intermittent renewable sources [5–8]. Of these products, C2 or higher hydrocarbons are preferred over products such as CO because they are either important industrial raw materials or high energy-density fuels [8,9].

Among the many metal cathode catalysts that have been investigated for reduction of CO_2, Cu is the only metal that catalyzes the production of short hydrocarbons at considerable high Faradaic efficiency (FE) [7–10]. However, the overpotentials for hydrocarbon production are usually high (0.7–1 V) on Cu electrodes, which reduces the energetic efficiency of the system [7,11–13]. Meanwhile, when using Cu the production rate is quite low under ambient conditions (current density typically less than 35 mA cm^{-2} at cathode potentials positive of −1 V *vs.* RHE) [9,12,14–18]. These challenges are mainly due to low catalyst activity as well as lack of ideal electrolysis conditions for this process. More active cathode catalysts as well as optimum electrolysis conditions are needed to make electroreduction of CO_2 a process to be considered as an efficient approach for energy storage from intermittent sources or for the synthesis of chemicals that are used as raw materials at scale.

Recently, significant improvements have been made towards achieving high performance in the reduction of CO_2 on Cu-based electrodes. Several studies have shown that oxide-derived Cu films or cubes exhibit substantial improvement in overpotential and selectivity for CO_2 reduction compared to plain Cu metal catalysts [12,16,18,19]. However, the overpotential for C_2H_4 production is still unacceptably large and the total current densities do not exceed 55 mA cm^{-2} at all applied potentials. A variety of electrolytes has been used, ranging in pH from neutral to alkaline [20,21]. A complication of CO_2 reduction under alkaline conditions is the reaction of KOH with CO_2 to form carbonates. Through the use of CO instead of CO_2 as the reactant, improved selectivity for C_2H_4 or C_2H_5OH formation could be observed under alkaline conditions [21,22]. However, an additional step would be needed to first reduce CO_2 to CO before further reduction of CO, making the whole process more complex while increasing energy consumption. Sammells et al. were able to overcome this issue by using a gas diffusion electrode (GDE), covered with Cu particles, to separate a stationary alkaline electrolyte solution (KOH) from the CO_2 reactant [20]. A total current density as high as 400 mA cm^{-2} was obtained to produce a mixture of CH_4 (9.1% FE) and C_2H_4 (69% FE), however, a relatively high cathode potential of −1.98 V *vs.* RHE had to be applied, probably due to the low activity of the Cu particles used.

Here, we report on the efficient electroreduction of CO_2 to C_2H_4 and C_2H_5OH at much lower overpotentials achieved with Cu nanoparticles (CuNPs) with high surface roughness deposited on GDEs in an alkaline flow electrolyzer. Remarkably, Cu catalysts deposited on GDEs exhibited relatively stable performance for 4 h under the alkaline condition. Here we investigate the effect of morphology (roughness) and the amount of Cu oxides present in the different catalysts on the observed product distribution and current density. Also, by comparing the performance of the Cu catalysts studied here to the performance of previously reported Cu catalysts [9,12,14–16,18,23], we elucidate reasons for the high production of ethylene and ethanol under remarkably mild conditions. Based on the observed trends in product distribution we suggest a reaction pathway for CO_2 reduction on CuNP catalysts.

2. Experimental

2.1. Preparation of CuNP catalysts

Four CuNP catalysts (Cu-1, Cu-2, Cu-3 and Cu-4) were synthesized at an ambient temperature using a solution based method in which solvent composition was varied in the absence or presence of citric acid [24–26]. The reaction solution was prepared by dissolving 3 mmol copper acetate (Wako) in 250 ml solvent. The black precipitates of CuNPs were immediately obtained after the addition of the $NaBH_4$ solution to the reaction solution regardless of the presence of citric acid, an additive known to enhance production of uniform nanoparticles [27,28]. The solvent and additive used for the preparation of each CuNPs are tabulated in Table 1. Prepared CuNPs were dried in vacuum. For comparison, a commercially available Cu (20–40 nm, Alfa Aesar, Cu-comm) was also used in this study. Detailed synthetic procedures for all the CuNP samples can be found in the Supplementary material.

2.2. Physical characterizations

X-ray powder diffraction (XRPD) measurements of the Cu catalysts were performed at room temperature using a Rigaku MiniFlex 600 ($\lambda = 1.54059$ Å, Cu-Kα). Lattice constants, crystallite sizes, and weight ratio of each phase in the five samples (Cu-1, Cu-2, Cu-3, Cu-4, and Cu-comm) were estimated by Rietveld analyses performed using a Topas software package (Bruker AXS Inc.). All patterns were successfully fitted using a combination of simulated patterns for Cu (with the space group of *Fm*-3*m*), Cu_2O (*Pn*-3*m*), and CuO (*C*2/*c*).

X-ray photoelectron spectroscopy (XPS) measurements of the Cu catalysts were performed at ambient temperature using PHI 5000 VersaProbe II (ULVAC-PHI Inc.) with Al-Kα X-ray source.

The morphologies of the Cu samples are examined using transmission electron microscopy (TEM, JOEL 2100 CRYO) operated at 200 kV. The TEM sample was prepared by suspending the catalyst in isopropanol and placing a drop of the suspension onto a holey carbon-coated 200 mesh grid followed by solvent evaporation overnight at room temperature.

2.3. Electrolyzer

An electrochemical flow cell reported previously [29–34] is used as the CO_2 electrolyzer. A schematic of the flow cell used in this study is shown in Fig. 1. In this work, an anion exchange membrane (Fumatech®) is inserted between the catholyte and anolyte chamber to prevent the liquid products from diffusing to the anode where they may get oxidized. Stainless steel plates (5.5 × 2.5 cm) serve as current collectors to hold the flow cell together via a squeeze-action toggle plier clamp (McMaster Carr

Table 1
Solvents and additives used for the preparation of Cu nanoparticles.

Samples	Solvent	Additive
Cu-1	2–ethoxyethanol	No
Cu-2	Water	No
Cu-3	Water	Citric acid (30 mmol)
Cu-4	2–ethoxyethanol/water (v/v: 50/50)	Citric acid (30 mmol)

5062A63) and provide electrical contact between the GDE and an external potentiostat (Autolab, PGSTAT-30, EcoChemie). Two 1.5-mm thick polyether ether ketone (PEEK) spacers with a precisely machined 0.5-cm wide by 2.0-cm long window provide the catholyte and anolyte flow fields, respectively. The cathode current collector has a precisely machined 0.5-cm wide by 2.0-cm long window with 0.5 cm depth behind the GDE to allow for the flow of gases. The anode is open to air, allowing oxygen to escape.

2.4. Electrodes preparation

The cathodes were prepared using an air-brush method as previously reported [33]. Cathode catalyst inks were prepared by mixing tetrahydrofuran (200 μL), catalyst (3.4 mg), Nafion® solution (4.4 μL, 5 wt%, Fuel Cell Earth), and isopropyl alcohol (200 μL). The inks were then sonicated (Vibra-Cell ultrasonic processor, Sonics & Materials) for 15 min and air-brushed [33] on a gas diffusion layer (GDL, Sigracet 35 BC, Ion Power) to create a GDE covered with catalyst over a geometric area of 2.5 × 0.8 cm^2. A PTFE spacer with a 2.5 × 0.8 cm^2 window was placed on top of GDL during the deposition process to avoid catalyst being deposited outside of the expected area on the GDL. The actual loading was determined by weighing the GDL before and after deposition. The weight loss was found to be on the order of 50% for the air-brushed cathodes since a fraction of the catalyst ended up on the spacer, or was left behind in the air-brush. The anodes were prepared by hand-painting of IrO_2 catalyst inks comprised of Millipore water (200 μL), IrO_2 catalyst (2.5 mg, non-hydrate, Alfa Aesar), Nafion® solution (6.5 μL, 5 wt%, Fuel Cell Earth), and isopropyl alcohol (200 μL) over a geometric area of 1.0 × 2.5 cm^2. Both the cathode and anode loading were determined to be 1.0 ± 0.1 mg cm^{-2}. A fresh cathode was used for each flow cell test.

2.5. Electrolysis and product analysis

The flow cell shown in Fig. 1 was used to perform the electrolysis of CO_2. A potentiostat (Autolab PGSTAT-30, EcoChemie) was used to control the cell potential (−1.6 V, −1.75 V, −2 V, −2.25 V, −2.5 V, −2.75 V, −3 V, −3.5 V) in the potentiostatic electrolysis mode to measure the activity of each catalyst [29]. For each potential, the cell was allowed to reach steady state, after which the gaseous product stream was analyzed using a gas chromatography (Thermo Finnegan Trace GC). The current at a given condition was obtained by averaging the current over 180 s before stepping to the next potential.

Individual electrode potentials were recorded using multimeters (AMPROBE 15XP-B) connected to each electrode and a reference electrode (Ag/AgCl; RE-5B, BASi) placed in the electrolyte exit stream. 1 M KOH (pH = 13.48) or 0.5 M $KHCO_3$ (pH = 8.35) was used as the catholyte, while 1 M KOH was used as the anolyte. The measured potentials (*vs.* Ag/AgCl) were converted to the RHE reference scale using E (*vs.* RHE) = E (*vs.* Ag/AgCl) + 0.209 V + 0.0591 V/pH × pH as previously reported [18,22]. The electrode potentials were corrected for iR drop as previously reported [32,35]. A mass flow controller (MASS-FLO®, MKS instrument) was used to set the CO_2 (S.J. Smith Welding Supply) flow rate at 7 SCCM. A syringe pump (PHD 2000, Harvard Apparatus) flowed the electrolyte to minimize boundary layer depletion effects and supply fresh electrolytes thereby helping to maintain the pH on the electrode surface. The flowing stream provides flexibility in operation conditions, minimizes water management issues at the electrodes, and facilitates online sample collection followed by product analysis [31]. The flow rate was set at 0.5 mL min^{-1} when applying cell potentials of −2 to −3.5 V as done previously [31], while a flow rate of 0.1 mL min^{-1} was used for cell potentials between −1.6 and −2 V to increase the concentration of the liquid products at low current density operation conditions. The pH of the electrolyte was measured using a calibrated pH meter (Thermo Orion, 9106BNWP). A pressure controller (Cole–Parmer, 00268TC) downstream from the cell was used to keep the gas pressure in cell lower than the atmosphere, allowing gas products formed on the catalyst surface of the GDE to leave through the GDE to the gas stream.

Periodically, for product analysis, 1 mL of the effluent gas stream was sampled automatically and diverted into a gas chromatograph (Thermo Finnegan Trace GC) equipped with both the thermal conductivity detection (TCD) and flame ionization detector (FID), with a Carboxen 1000 column (Supelco) and Helium as the carrier gas at a flow rate of 20 SCCM. Meanwhile, the exit catholyte was collected at each applied potential and analyzed using ^1H NMR technique reported previously [17,36,37]. 100 μL of the catholyte was mixed with 400 μL D_2O (99.9% deuterium atom, Sigma–Aldrich) and 100 μL of an internal standard consisting of 1.25 mM DMSO (99.98%, Calbiochem) in D_2O. The results presented here are from 32 scans (UI500NB, Varian) after solvent suppression, and processed using the MestReNova software (MestReLab).

For the long-term electrolysis, we controlled the total current in the galvanostatic electrolysis mode. In the galvanostatic mode, the flow cell was tested at total current of −150 mA. Cathode potential was recorded every 15 min and products were analyzed every 1 h.

The onset potential is defined as the lowest cathode potential at which we observe gas products in GC or liquid products from NMR.

The Faradaic efficiency for a specific product is calculated using the following equation:

$$\varepsilon_{Faradaic} = \frac{z \cdot n \cdot F}{Q}$$

where

z = the number of electrons exchanged (for example, $z = 2$ for reduction of CO_2 to CO)
n = the number of moles for a specific product
F = Faraday's constant ($F = 96485$ C/mol)

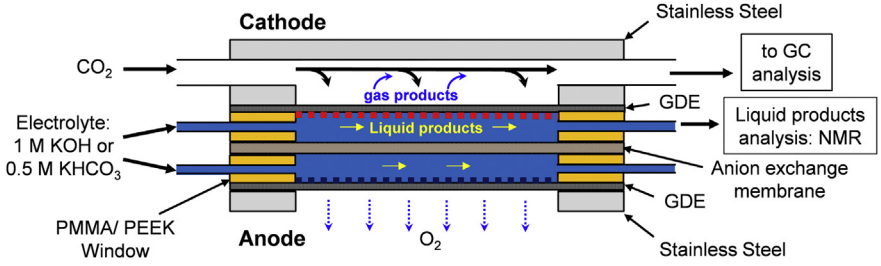

Fig. 1. Schematic representation of the electrochemical flow cell used in this study.

Q = the charge passed (C)

The partial current density for a specific product equals total current density multiplies Faradaic efficiency for this product.

2.6. Relative surface roughness measurement

The relative surface roughness factor of each catalyst was determined by the double-layer capacitance [12,38] in a three standard electrode cell with a catalyst-covered 3-mm glassy carbon rotating disk electrode (RDE; Metrohm 6.1204.300) as the working electrode, a Pt gauze (100 mesh, 99.9% metals basis, Sigma–Aldrich, 25*25 mm^2) as the counter electrode, and a Ag/AgCl as the reference electrode (RE-5B, BASi). The cyclic voltammetry (CV) was measured in an Ar-saturated 0.1 M $HClO_4$ aqueous solution. Catalyst ink was prepared using the same method as described above. 4 μL catalyst ink was deposited on the RDE and then dried under flowing Ar. The CV was measured in the potential range of −0.41 to −0.1 V (vs. Ag/AgCl), where only double-layer charging/discharging occurs. The capacitance is the slope from the plot of current density *vs.* scan rate.

3. Results and discussion

3.1. Composition, structure and morphology analysis

XRPD was used to characterize the structure and composition of solid phases formed in the catalysts. The XRPD patterns of the as-synthesized CuNP catalysts Cu-1 to Cu-4 as well as the commercial sample (Cu-comm) are shown in Fig. 2a. All synthesized Cu catalysts are composed of Cu and Cu_2O, but in different relative amounts. The Cu-comm sample also contains a fraction of CuO. The presence of CuO is also evident from the characteristic shake-up peaks at 940 eV and 944 eV [39] in the XPS pattern shown in Fig. 2b. Small shake-up peaks were also found for Cu-2. However, the characteristic peak for CuO is absent in the XRPD pattern for Cu-2, probably because only a very small amount of CuO is present on its surface. Rietveld analysis of the XRPD patterns determined the specific composition and crystallite size of each sample (results summarized in Table 2, final fit plots combined in Fig. S1). Cu-1 and Cu-3 have a lower amount of Cu_2O, while Cu-2 and Cu-4 contain a higher amount of Cu_2O. This result suggests that the use of 2–ethoxyethanol (as used in the synthesis of Cu-1) and citric acid (as used in the synthesis of Cu-3) helps prevent oxidation, while use of a water/2–ethoxyethanol mixture increases the oxidation of Cu. Cu is known to oxidize to Cu_2O under ambient condition [9,39], but the extent of oxidation is affected by the synthetic conditions, as shown in this study. Further analysis of the XRPD data using the Scherrer equation indicates that Cu-3 is composed of smaller crystallites than the other samples, presumably a consequence of the use of citric acid as an additive. In the preparation of Cu-4 citric acid is also used as an additive, resulting in larger crystallites in Cu-4 compared to those in Cu-3. This difference is probably due to the presence of 2–ethoxyethanol in the solvent mixture used for the preparation of Cu-4, with the additional 2–ethoxyethanol decreasing the solubility of citric acid and therefore its dispersion into the solvent during synthesis.

The morphologies of the five samples were characterized using TEM (Fig. 3). The catalysts exhibited very different morphological features: The Cu-1, Cu-2, and Cu-3 catalysts are comprised of irregular particle shapes with interconnected nanocrystalline networks and grain boundaries, while the Cu-4 and Cu-comm samples mostly feature spherical particles that overlap with each other. TEM histograms of the five Cu catalysts are summarized in Fig. S2 (Supplementary material). The particle size of Cu-comm sample is non-uniform, ranging from about 5 nm to 90 nm. In contrast, the particles of the four synthesized catalysts are more uniform and smaller, in the 10–50 nm range. Comparing the TEM results with the XRPD results reveals that the average particle size of Cu-1, Cu-2, and Cu-3 from TEM (~20–30 nm) is significantly bigger than the crystallite size determined from analysis of the XRPD patterns using the Scherrer equation (~5–15 nm). This discrepancy can probably be attributed to the fact that each particle in Cu-1, Cu-2, and Cu-3 is comprised of several crystallites. For the Cu-comm and Cu-4 samples the particle sizes obtained from TEM are similar to the crystallite sizes obtained from XRPD analysis.

The relative surface roughness factor of each catalyst was determined by CV measurement of the double-layer capacitance for each sample. If we assume the surface roughness factor for Cu-comm to be 1, then the relative surface roughness factors for other Cu catalysts are calculated according to their double-layer capacitances (Fig. S3 in the Supplementary material). The results of double-layer capacitances as well as the surface roughness factors for all the catalysts (Table 3) reveal that catalysts Cu-1, 2, 3 have rougher surfaces than catalysts Cu-4 and Cu-comm.

3.2. CO_2 electrolysis

We compared the activities of the Cu catalysts towards CO_2 electrolysis in the flow cell described above. Single electrode

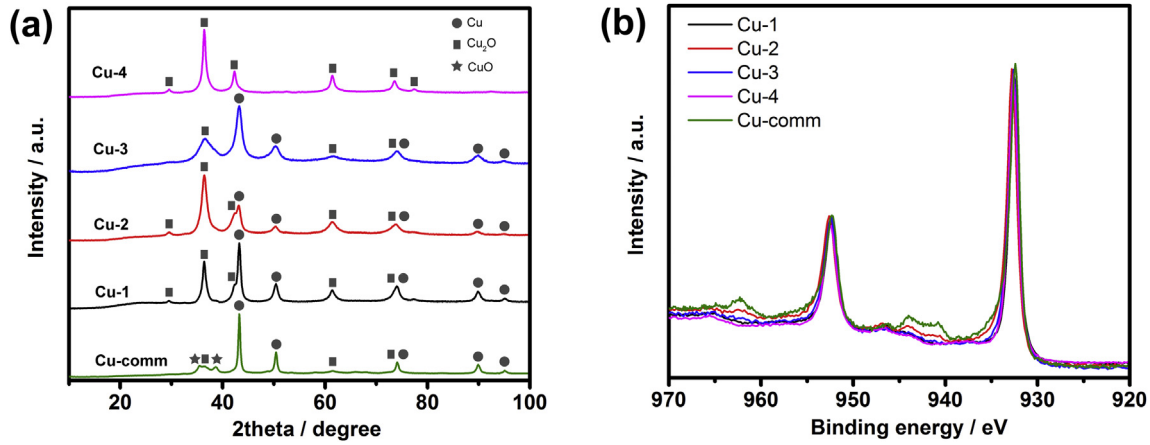

Fig. 2. (a) XRD patterns of the four synthesized Cu nanoparticles and commercially obtained Cu nanoparticles (Cu-comm); and (b) XPS high resolution scans of the Cu 2p peaks of the five samples.

Table 2
Refined parameters of Rietveld analyses for the five samples.

	Lattice parameter (Å)	Crystallite size (nm)	Lattice parameter (Å)	Crystallite size (nm)	R_{wp}	R_p
Cu-1	Cu(fcc): 47.8%		Cu_2O: 52.2%		2.67	1.88
	3.6161 ± 0.0004	15.3 ± 0.2	4.2645 ± 0.0006	10.1 ± 0.1		
Cu-2	Cu(fcc): 13.9%		Cu_2O: 86.1%		2.12	1.64
	3.6251 ± 0.0003	12.3 ± 0.3	4.2705 ± 0.0002	7.2 ± 0.1		
Cu-3	Cu(fcc): 42.8%		Cu_2O: 57.2%		1.94	1.34
	3.6219 ± 0.0009	7.9 ± 0.1	4.242 ± 0.002	3.1 ± 0.1		
Cu-4	Cu(fcc): 2.2%		Cu_2O: 97.8%		2.28	1.64
	3.595 ± 0.003	12.5 ± 2	4.2679 ± 0.0005	11.8 ± 0.1		
Cu-comm	Cu(fcc): 47.6%		Cu_2O: 26.7%		1.88	1.29
	3.6155 ± 0.0002	25.9 ± 0.2	4.2515 ± 0.0009	4.9 ± 0.1		
	CuO: 25.7%					
	a = 4.681 ± 0.003, b = 3.432 ± 0.002, c = 5.133 ±0.004, β = 99.25 ± 0.04°	9.1 ± 0.2				

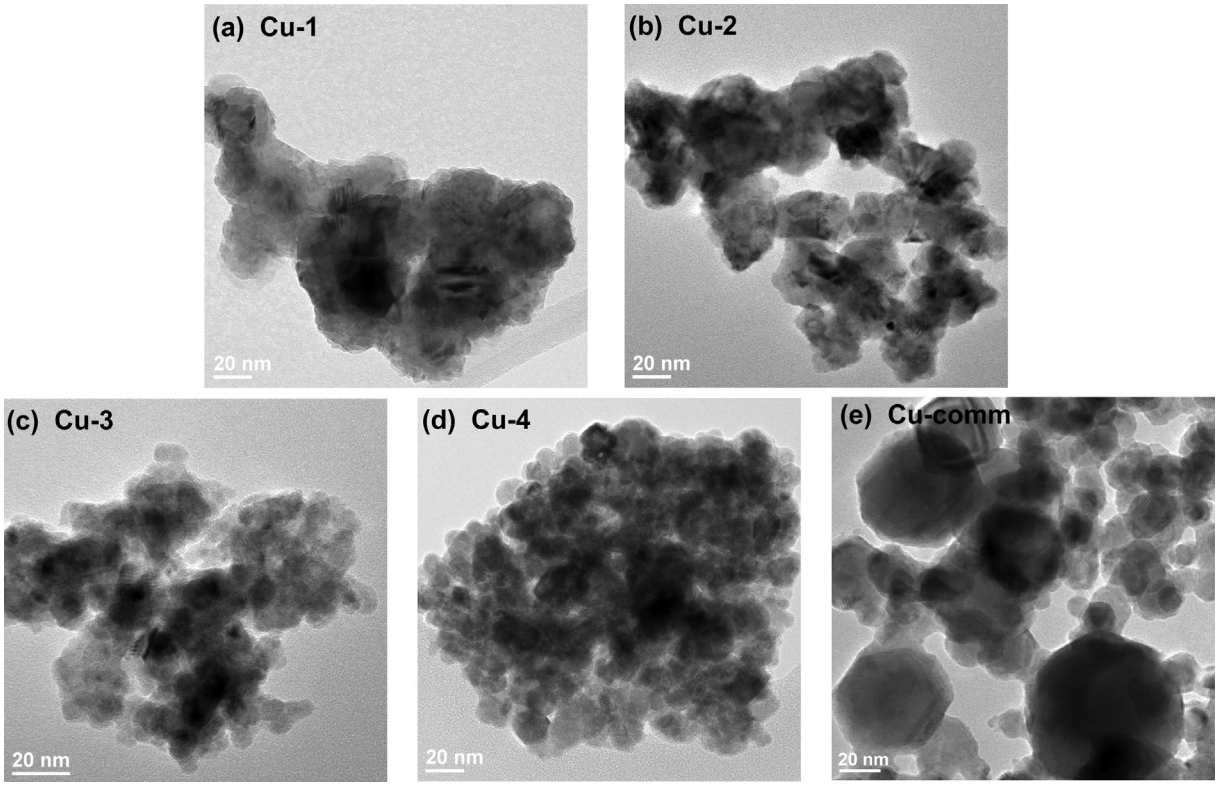

Fig. 3. TEM micrographs of the Cu catalysts: (a) Cu-1; (b) Cu-2; (c) Cu-3; (d) Cu-4; (e) Cu-comm.

polarization curves (electrode potentials plotted against the total current density) from each sample measurement are summarized in Fig. 4. All electrode potentials are reported with respect to RHE and are iR-corrected as previously reported [32]. Current densities are calculated based on geometric surface area of the electrode. As shown in Fig. 4, the Cu-1, 2, 3 catalysts achieve higher total current densities than Cu-4 and Cu-comm, which is in agreement with the measured trends in relative surface roughness: a rougher catalyst

surface results in higher total current density.

The FE and partial current density for all major products (CO, H_2, C_2H_4, and C_2H_5OH) using all Cu samples in 1 M KOH are plotted as a function of cathode potential in Fig. 5. Specific values for cathode potential, total current densities and Faradaic efficiencies for all products are listed in Table S1 (Supplementary material). Fig. 5a and c show that Cu-1, Cu-2, and Cu-3 achieve higher FE for CO and lower FE for H_2 than Cu-4 and Cu-comm. Although Cu-1, Cu-2, and Cu-3 contain different amount of oxides, their FEs for CO and H_2 are almost identical, suggesting that Cu_2O was first reduced to metallic Cu before CO_2 reduction, similar to previously reported work [18,19]. The effect of the initial amount of oxide in each of the samples on product distribution seems minimal. The differences in selectivity for CO and H_2 observed for the different catalysts probably can be attributed to differences in morphology.

In this study, relatively high FEs and partial current densities for C_2H_4 and C_2H_5OH are achieved at low cathode overpotentials. For all Cu samples, the FEs for C_2H_4 are in the range of 27%–46% (Fig. 5e), while the FEs for C_2H_5OH are in the range of 7%–17% (Fig. 5g). The observed significant Faradaic efficiencies for C_2H_4 and C_2H_5OH is probably due to the formation of newly reduced Cu surfaces composed of favorable steps and edges. These steps and edges with under-coordinated Cu atoms are known to be selective for C_2H_4 and C_2H_5OH formation as they promote the adsorption of C1 intermediates and facilitate their dimerization [9,15,18,19]. Compared with polycrystalline Cu foils, rough CuNPs may have a larger concentration of these steps and edges [9], as well as high-index crystal surfaces [7,40], which are favorable for C_2H_4 and C_2H_5OH formation. While similar FEs for C_2H_4 have been reported previously, here these FEs are achieved at overpotentials in the range of 0.66–0.87 V, which is at least 0.20 V–1 V lower than the overpotentials needed to achieve the same FE for C_2H_4 in the aforementioned prior work [9,14,16,18,20,21,23]. The partial current densities for C_2H_4 and C_2H_5OH on the Cu-1 electrode are -150 mA cm^{-2} (Fig. 5f) and -48 mA cm^{-2} (Fig. 5h), respectively, at -0.58 V *vs.* RHE. These values are at least one order of magnitude higher than most previously reported partial current densities for C_2H_4 and C_2H_5OH on Cu electrodes evaluated at similar potentials under ambient conditions [9,12,14,16–18,23,41]. The use of GDEs minimizes CO_2 mass transfer limitations and enables better control of the three-phase interface where the reactions take place. The use of alkaline electrolyte (as opposed to often used neutral electrolytes such as $KHCO_3$ or KCl) minimizes ohmic resistance of the electrolyte. Together, these two factors explain the one order of magnitude improvement in current density. We also found that the FEs for C_2H_4 and C_2H_5OH are similar for all the five Cu catalysts (Fig. 5e and g). This is probably due to the formation of similar amounts of steps and edges with under-coordinated Cu atoms on all five catalysts upon application of the reducing potentials.

For all catalysts, the FE for CO decreased from -0.3 V to -0.5 V, while C_2H_4 and C_2H_5OH started to be produced in the same potential range (Fig. 5a, e, and g). This trend implies that adsorbed CO is an important intermediate for electroreduction of CO_2 before it is further reduced to hydrocarbons such as C_2H_4 and C_2H_5OH, as suggested previously by others [7,11,17,42]. Based on the high FEs for C2 products observed in this work, as well as information from prior work [17,18,42–44], a possible reaction pathway (Fig. 6) that favors C2 products over CH_4 is proposed. Adsorbed CO is first formed after two steps of proton and electron transfer. Moderately adsorbed CO species then are hydrogenated to adsorbed CHO, COH, or C species, of which CHO is mainly converted to CH_4, while COH and C are mainly converted to C_2H_4 or C_2H_5OH through the dimerization of CH_2 or insertion of CO, respectively. We postulate that the much lower Faradaic efficiency for CH_4 (<2%) compared to the Faradaic efficiency for C2 products (~50%) in this study can be explained by the relative low amounts of adsorbed CHO intermediate compared to the amount of adsorbed COH or C intermediates. This proposed pathway lacks direct dimerization of adsorbed CO because prior work suggests that this step is kinetically unfavorable compared with the dimerization of hydrogenated species [45].

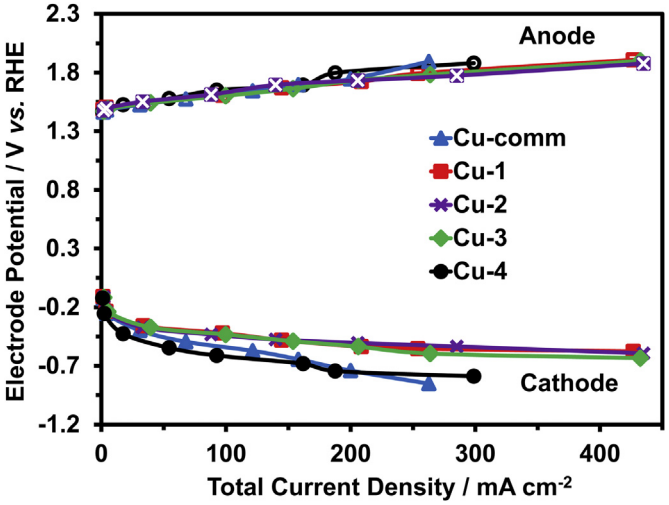

Fig. 4. iR-corrected single electrode polarization curves of the experiments using five Cu catalysts: Cu-1, Cu-2, Cu-3, Cu-4 and Cu-comm. Electrolyte: 1 M KOH.

Table 3
Capacitance and surface roughness factors for Cu catalysts in this work.

Catalysts	Capacitance (mF)	Surface roughness factor
Cu-1	0.57	1.5
Cu-2	0.52	1.4
Cu-3	0.52	1.4
Cu-4	0.43	1.2
Cu-comm	0.37	1

3.3. Comparison to prior work

To further study the benefit of alkaline electrolyte, and to allow for better comparison with prior work, we also tested the Cu-1 catalyst using 0.5 M $KHCO_3$ as the catholyte. Fig. 7 presents our data obtained using Cu-1 in both 1 M KOH and 0.5 M $KHCO_3$, as well as data sets from previous CO_2 reduction studies that used a Cu-based cathode catalyst [9,12,14–16,18,23]. Most of the previous studies used CuNPs as catalysts in close to neutral electrolytes such as $KHCO_3$, $NaHCO_3$, and $KClO_4$ [9,14,15,18,23,46,47], while other studies used oxide-derived Cu materials [12,16]. Specific information on the catalyst, electrolyte and cell configuration in each of the previous reports can be found in Table 4. An earlier onset is observed for all major products when using Cu-1 in KOH instead of other catalysts and/or electrolytes (Fig. 7). Specifically for hydrocarbon production, Cu-1 exhibits improvements of 140 mV and 80 mV in overpotential for CO_2 reduction to C_2H_4 and C_2H_5OH, respectively, compared to prior data (Fig. 7c and d) [12,16]. This improvement is probably due to the faster reaction kinetics when using alkaline electrolyte [19,22,32], which is further supported by the fact that conducting the experiment in 0.5 M $KHCO_3$ does not show similar improvements in the onset potential. The FEs observed for H_2 when using Cu-1 in KOH are below 22%, which is much lower than typical levels reported previously (Fig. 7b). However, when using Cu-1 the FEs for H_2 are higher in $KHCO_3$

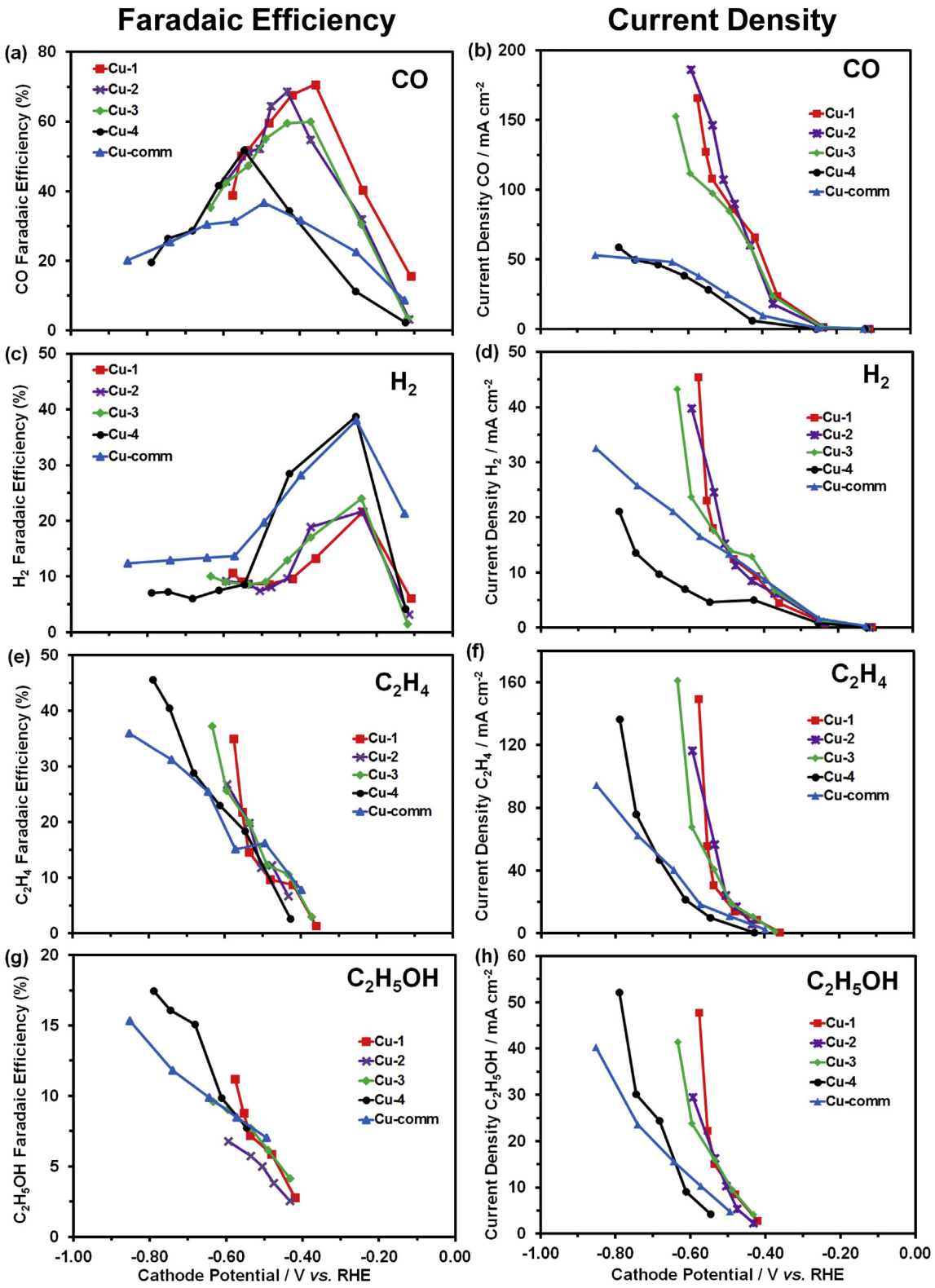

Fig. 5. Faradaic efficiencies as well as corresponding partial current densities for CO (a,b), H_2 (c,d), C_2H_4 (e,f), and C_2H_5OH (g,h). Electrolyte: 1 M KOH. Each data point represents the average of three measurements.

electrolyte than when using KOH as the electrolyte. This drop in FE for H_2 can be attributed to the much lower H^+ concentration when using alkaline electrolyte [32]. Cu-2, Cu-3, Cu-4 and Cu-comm exhibit similar trends with respect to the suppression of hydrogen evolution when used in $KHCO_3$ *vs.* KOH (data not shown).

3.4. Durability measurement

We also compared the durability of the Cu-1 and the Cu-comm catalysts under electrolysis conditions (galvanostatic mode, at a constant current of −150 mA). Fig. 8 indicates that the cathode

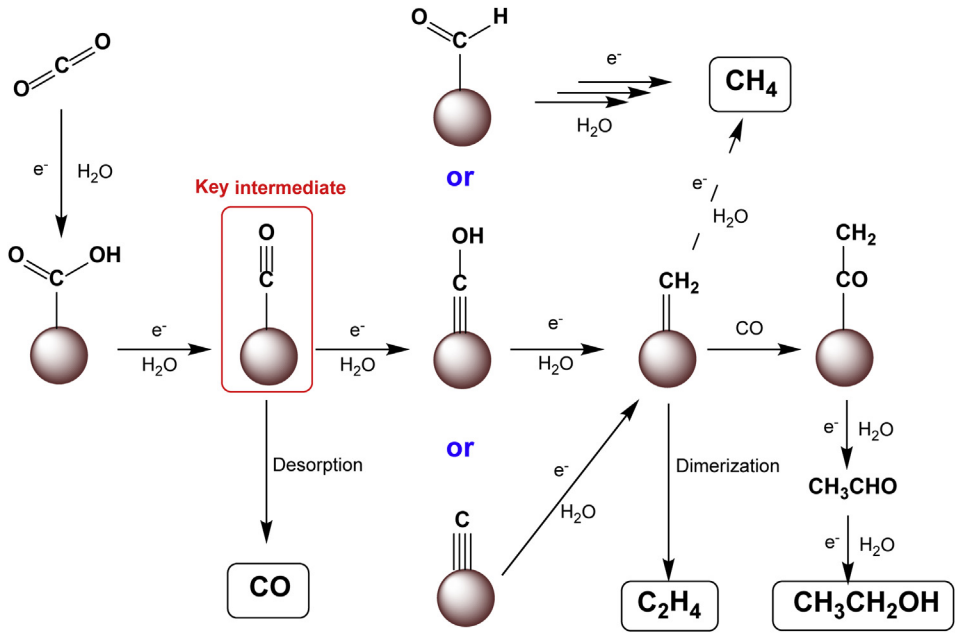

Fig. 6. Proposed reaction pathway for the CO_2 reduction to various products (mainly C_2H_4 and C_2H_5OH) on Cu nanoparticles. Dashed line with arrows indicates the step that is less likely to happen.

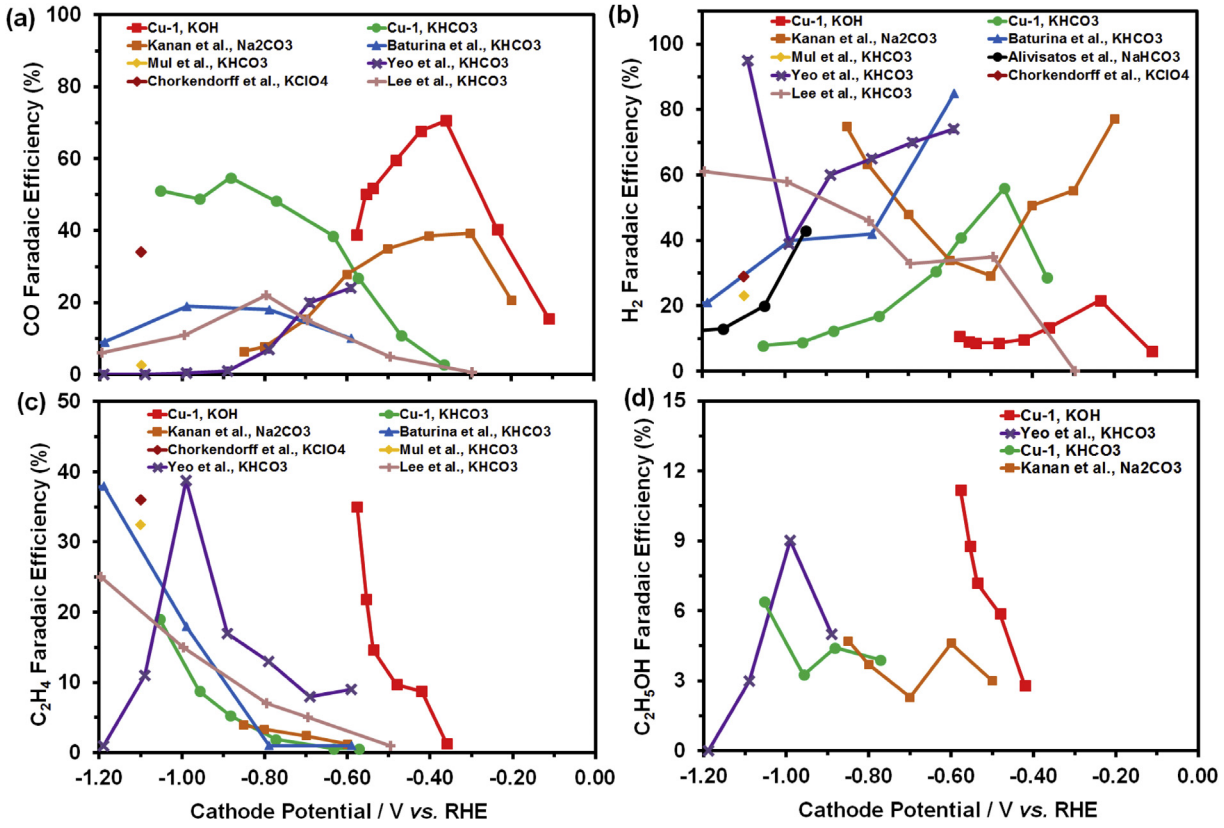

Fig. 7. The Faradaic efficiencies of this study when using 1 M KOH (red curves) or 0.5 M $KHCO_3$ (green curves) compared to those obtained in prior work using Cu-based cathode catalysts [9,12,14–16,18,23]. (For interpretation of the references to colour in this figure legend, the reader is referred to the web version of this article.)

potential remains stable for both catalysts over 4-hr electrolysis test. Similarly, only very small changes in product distribution were observed. This data suggest that both Cu-1 and Cu-comm exhibit significant stability under electrolysis conditions, but longer experiments are needed to determine their durability over extended periods of time.

4. Conclusions

In summary, we report high conversion of CO_2 to C_2H_4 and

Table 4
A summary of experimental conditions used in several previous reports of carbon dioxide conversion using copper-based catalysts.

Sample name	Catalyst	Electrolyte	pH	Cell Configuration	Ref in the main text
Alivisatos et al., $NaHCO_3$	Cu nanoparticle	0.1 M $NaHCO_3$	6.8	Two compartment flow cell	[15]
Baturina et al., $KHCO_3$	Cu nanoparticle	0.1 M $KHCO_3$	6.8	Standard RDE set-up	[23]
Chorkendorff et al., $KClO_4$	Cu nanoparticle	0.1 M $KClO_4$	6	Standard 3-electrode cell	[9]
Kanan et al., Na_2CO_3	Cu_2O derived electrode	0.5 M Na_2CO_3	7.2	Two compartment cell	[12]
Yeo et al., $KHCO_3$	Cu_2O derived films	0.1 M $KHCO_3$	6.8	Two compartment cell	[18]
Mul et al., $KHCO_3$	Cu nanoparticle	0.1 M $KHCO_3$	6.8	Standard 3-electrode cell	[14]
Lee et al., $KHCO_3$	Cu_2O/Cu	0.5 M $KHCO_3$	N.P.	H-type electrolytic cell	[16]

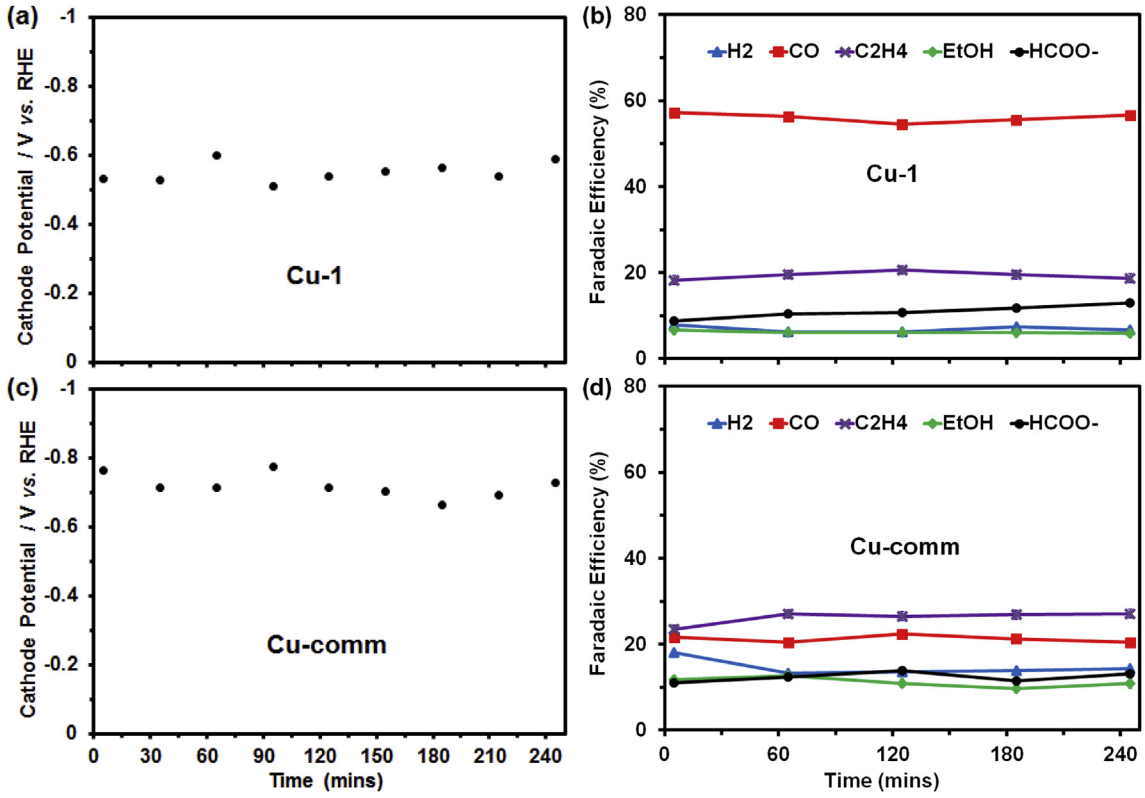

Fig. 8. (a), (c) Cathode potential and (b), (d) Faradaic efficiency as a function of time when using Cu-1 or Cu-comm as the catalyst in a galvanostatic experiment (current kept contestant at −150 mA) over a total of 4 h.

C_2H_5OH using active CuNP catalysts in a single alkaline electrolyzer in this work. Compared to prior studies, significantly higher partial current densities for C_2H_4 (as high as -150 mA cm^{-2}) and C_2H_5OH (as high as -48 mA cm^{-2}) in combination with lower overpotentials (at least 140 mV lower for C_2H_4 production and 80 mV lower for C_2H_5OH production) were obtained for the Cu-1 catalyst in alkaline electrolyte. The high current densities are attributed to the use of GDEs covered with high surface roughness Cu catalysts and the use of alkaline electrolyte in the flow cell (lower ohmic resistance), while the decreased overpotential is attributed to the use of active CuNP catalysts in combination with improved kinetics due to the alkaline pH.

We also found that catalyst morphology rather than the amount of surface oxide affects the product distribution. However, whether reconstructing of the catalyst upon applying a reducing potential [48] plays a role in this system is unclear. Further investigations using *in situ* microscopic techniques would potentially reveal structural transformation of the CuNPs under electrolysis conditions. Also, further mechanistic studies, both in an experimental and computational context, could further elucidate the reaction mechanisms and differences in kinetics associated with use of alkaline electrolyte.

Acknowledgment

We gratefully acknowledge the support of the International Institute for Carbon-Neutral Energy Research (WPI–I2CNER), sponsored by the Japanese Ministry of Education, Culture, Sports, Science and Technology. This work was also partially supported by JST-CREST and JSPS KAKENHI Grants 25288030, 24655040, 24850013 and 21350031. SM acknowledges support from FMC Educational Fund for a FMC Graduate Fellowship.

Appendix A. Supplementary data

Supplementary data related to this article can be found at http://dx.doi.org/10.1016/j.jpowsour.2015.09.124.

References

[1] S. Pacala, R. Socolow, Science 305 (2004) 968–972.
[2] P. Taylor, Energy Technology Perspectives, International Energy Agency, 2010.
[3] T. Matsumoto, M. Sadakiyo, M.L. Ooi, S. Kitano, T. Yamamoto, S. Matsumura, K. Kato, T. Takeguchi, M. Yamauchi, Sci. Rep. 4 (2014).
[4] R. Watanabe, M. Yamauchi, M. Sadakiyo, R. Abe, T. Takeguchi, Energy Environ. Sci. 8 (2015) 1456–1462.

[5] H.-R.M. Jhong, S. Ma, P.J.A. Kenis, Curr. Opin. Chem. Eng. 2 (2013) 191–199.
[6] D.T. Whipple, P.J.A. Kenis, J. Phys. Chem. Lett. 1 (2010) 3451–3458.
[7] Y. Hori, Electrochemical CO_2 reduction on metal electrodes, in: C. Vayenas, R. White, M. Gamboa-Aldeco (Eds.), Modern Aspects of Electrochemistry, Springer, New York, 2008, pp. 89–189.
[8] M. Gattrell, N. Gupta, A. Co, J. Electroanal. Chem. 594 (2006) 1–19.
[9] W. Tang, A.A. Peterson, A.S. Varela, Z.P. Jovanov, L. Bech, W.J. Durand, S. Dahl, J.K. Norskov, I. Chorkendorff, Phys. Chem. Chem. Phys. 14 (2012) 76–81.
[10] Y. Hori, H. Wakebe, T. Tsukamoto, O. Koga, Electrochim. Acta 39 (1994) 1833–1839.
[11] A.A. Peterson, F. Abild-Pedersen, F. Studt, J. Rossmeisl, J.K. Norskov, Energy Environ. Sci. 3 (2010) 1311–1315.
[12] C.W. Li, M.W. Kanan, J. Am. Chem. Soc. 134 (2012) 7231–7234.
[13] R. Reske, H. Mistry, F. Behafarid, B. Roldan Cuenya, P. Strasser, J. Am. Chem. Soc. 136 (2014) 6978–6986.
[14] R. Kas, R. Kortlever, A. Milbrat, M.T.M. Koper, G. Mul, J. Baltrusaitis, Phys. Chem. Chem. Phys. 16 (2014) 12194–12201.
[15] K. Manthiram, B.J. Beberwyck, A.P. Alivisatos, J. Am. Chem. Soc. 136 (2014) 13319–13325.
[16] D. Kim, S. Lee, J.D. Ocon, B. Jeong, J.K. Lee, J. Lee, Phys. Chem. Chem. Phys. 17 (2015) 824–830.
[17] K.P. Kuhl, E.R. Cave, D.N. Abram, T.F. Jaramillo, Energy Environ. Sci. 5 (2012) 7050–7059.
[18] D. Ren, Y. Deng, A.D. Handoko, C.S. Chen, S. Malkhandi, B.S. Yeo, ACS Catal. 5 (2015) 2814–2821.
[19] F.S. Roberts, K.P. Kuhl, A. Nilsson, Angew. Chem. 127 (2015) 5268–5271.
[20] R.L. Cook, R.C. MacDuff, A.F. Sammells, J. Electrochem. Soc. 137 (1990) 607–608.
[21] Y. Hori, A. Murata, R. Takahashi, J. Chem. Soc. Faraday Trans. 1 (85) (1989) 2309–2326.
[22] C.W. Li, J. Ciston, M.W. Kanan, Nature 508 (2014) 504–507.
[23] O.A. Baturina, Q. Lu, M.A. Padilla, L. Xin, W. Li, A. Serov, K. Artyushkova, P. Atanassov, F. Xu, A. Epshteyn, T. Brintlinger, M. Schuette, G.E. Collins, ACS Catal. 4 (2014) 3682–3695.
[24] M. Yamauchi, T. Tsukuda, Dalton Trans. 40 (2011) 4842–4845.
[25] M. Yamauchi, K. Okubo, T. Tsukuda, K. Kato, M. Takata, S. Takeda, Nanoscale 6 (2014) 4067–4071.
[26] J.S. Bradley, G.H. Via, L. Bonneviot, E.W. Hill, Chem. Mater. 8 (1996) 1895–1903.
[27] S. Maheswari, P. Sridhar, S. Pitchumani, Electrocatalysis 3 (2012) 13–21.
[28] J. Guo, A. Hsu, D. Chu, R. Chen, J. Phys. Chem. C 114 (2010) 4324–4330.
[29] S. Ma, Y. Lan, G.M.J. Perez, S. Moniri, P.J.A. Kenis, Chemsuschem 7 (2014) 866–874.
[30] C.E. Tornow, M.R. Thorson, S. Ma, A.A. Gewirth, P.J.A. Kenis, J. Am. Chem. Soc. 134 (2012) 19520–19523.
[31] D.T. Whipple, E.C. Finke, P.J.A. Kenis, Electrochem. Solid-State Lett. 13 (2010) B109–B111.
[32] S. Ma, R. Luo, S. Moniri, Y. Lan, P.J.A. Kenis, J. Electrochem. Soc. 161 (2014) F1124–F1131.
[33] H.-R.M. Jhong, F.R. Brushett, P.J.A. Kenis, Adv. Energy Mater. 3 (2013) 589–599.
[34] M.R. Thorson, K.I. Siil, P.J.A. Kenis, J. Electrochem. Soc. 160 (2013) F69–F74.
[35] M.S. Naughton, A.A. Moradia, P.J.A. Kenis, J. Electrochem. Soc. 159 (2012) B761–B769.
[36] J. Wu, F.G. Risalvato, P.P. Sharma, P.J. Pellechia, F.-S. Ke, X.-D. Zhou, J. Electrochem. Soc. 160 (2013) F953–F957.
[37] C.S. Chen, A.D. Handoko, J.H. Wan, L. Ma, D. Ren, B.S. Yeo, Catal. Sci. Technol. 5 (2015) 161–168.
[38] M. Fan, Z. Bai, Q. Zhang, C. Ma, X.-D. Zhou, J. Qiao, RSC Adv. 4 (2014) 44583–44591.
[39] M. Yin, C.-K. Wu, Y. Lou, C. Burda, J.T. Koberstein, Y. Zhu, S. O'Brien, J. Am. Chem. Soc. 127 (2005) 9506–9511.
[40] Y. Hori, I. Takahashi, O. Koga, N. Hoshi, J. Phys. Chem. B 106 (2001) 15–17.
[41] S. Sen, D. Liu, G.T.R. Palmore, ACS Catal. 4 (2014) 3091–3095.
[42] K.J.P. Schouten, Y. Kwon, C.J.M. van der Ham, Z. Qin, M.T.M. Koper, Chem. Sci. 2 (2011) 1902–1909.
[43] Y. Hori, R. Takahashi, Y. Yoshinami, A. Murata, J. Phys. Chem. B 101 (1997) 7075–7081.
[44] R. Kas, R. Kortlever, H. Yılmaz, M.T.M. Koper, G. Mul, ChemElectroChem 2 (2015) 354–358.
[45] J.H. Montoya, A.A. Peterson, J.K. Nørskov, ChemCatChem 5 (2013) 737–742.
[46] Y. Lan, C. Gai, P.J.A. Kenis, J. Lu, ChemElectroChem 1 (2014) 1577–1582.
[47] J. Qiao, M. Fan, Y. Fu, Z. Bai, C. Ma, Y. Liu, X.-D. Zhou, Electrochim. Acta 153 (2015) 559–565.
[48] K.J. Lange, P.-C. Sui, N. Djilali, J. Electrochem. Soc. 157 (2010) B1434–B1442.